Impact of electron correlations on two-particle charge response in electron- and hole-doped cuprates

Abhishek Nag,[1,2,3,*] Luciano Zinni,[4] Jaewon Choi,[1,5] J. Li,[1,6] Sijia Tu,[7,8] A. C. Walters,[1] S. Agrestini,[1] S. M. Hayden,[9] Matías Bejas,[10] Zefeng Lin,[7,8] H. Yamase,[11] Kui Jin,[7,8] M. García-Fernández,[1] J. Fink,[12,13,†] Andrés Greco,[10,‡] and Ke-Jin Zhou[1,§]

[1]*Diamond Light Source, Harwell Campus, Didcot OX11 0DE, United Kingdom*
[2]*SwissFEL, Paul Scherrer Institute, 5232, Villigen-PSI, Switzerland*
[3]*Department of Physics, Indian Institute of Technology Roorkee, Uttarakhand 247667, India*
[4]*Facultad de Ciencias Exactas, Ingeniería y Agrimensura (UNR), Avenida Pellegrini 250, 2000, Rosario, Argentina*
[5]*Department of Physics, Korea Advanced Institute of Science and Technology (KAIST), 291 Daehak-ro, Daejeon 34141, Republic of Korea*
[6]*National Synchrotron Light Source II, Brookhaven National Laboratory, Upton, New York 11973, USA*
[7]*Beijing National Laboratory for Condensed Matter Physics, Institute of Physics, Chinese Academy of Sciences, Beijing 100190, China*
[8]*University of Chinese Academy of Sciences, Beijing 100049, China*
[9]*H. H. Wills Physics Laboratory, University of Bristol, Bristol BS8 1TL, United Kingdom*
[10]*Facultad de Ciencias Exactas, Ingeniería y Agrimensura and Instituto de Física Rosario (UNR-CONICET), Avenida Pellegrini 250, 2000, Rosario, Argentina*
[11]*Research Center for Materials Nanoarchitectonics (MANA), National Institute for Materials Science (NIMS), Tsukuba 305-0047, Japan*
[12]*Leibniz Institute for Solid State and Materials Research Dresden, Helmholtzstr. 20, D-01069 Dresden, Germany*
[13]*Institut für Festkörperphysik, Technische Universität Dresden, D-01062 Dresden, Germany*

(Received 20 July 2024; accepted 6 November 2024; published 21 November 2024)

Estimating many-body effects that deviate from an independent particle approach has long been a key research interest in condensed matter physics. Layered cuprates are prototypical systems, where electron-electron interactions are found to strongly affect the dynamics of single-particle excitations. It is, however, still unclear how the electron correlations influence charge excitations, such as plasmons, which have been variously treated with either weak or strong correlation models. In this work, we demonstrate the hybridized nature of collective valence charge fluctuations leading to dispersing acoustic-like plasmons in hole-doped $La_{1.84}Sr_{0.16}CuO_4$ and electron-doped $La_{1.84}Ce_{0.16}CuO_4$ using the two-particle probe, resonant inelastic x-ray scattering. We then describe the plasmon dispersions in both systems, within both the weak-coupling mean-field random phase approximation (RPA) and strong-coupling *t-J-V* model in a large-*N* scheme. The *t-J-V* model, which includes the correlation effects implicitly, accurately describes the plasmon dispersions as resonant excitations outside the single-particle intraband continuum. In comparison, a quantitative description of the plasmon dispersion in the RPA approach is obtained only upon explicit consideration of renormalized electronic band parameters. Our comparative analysis shows that electron correlations significantly impact the low-energy plasmon excitations across the cuprate doping phase diagram, even at long wavelengths. Thus, complementary information on the evolution of electron correlations, influenced by the rich electronic phases in condensed matter systems, can be extracted through the study of two-particle charge response.

DOI: 10.1103/PhysRevResearch.6.043184

I. INTRODUCTION

Interactions among constituent entities leading to emergent phenomena are observed across disciplines, including superconductivity [1,2], active colloids [3], and neural functions [4]. In condensed matter systems, dynamic behavior of the constituent entities is probed using spectroscopic techniques. For instance, in many-electron systems where electron-electron interactions dominate the low-energy physical properties, angle-resolved photoemission (ARPES) or tunneling spectroscopy can assess the strength of "electron correlation." These correlation effects arise from short-range interactions between particles, which are seen in the low-energy quasi-particle properties. The direct observation of dynamical charge susceptibility, representing the two-particle charge-charge correlation function $\chi_c''(\mathbf{q}, \omega)$, in comparison, is possible via spectroscopic techniques such as resonant inelastic x-ray scattering (RIXS) or electron energy-loss spectroscopy (EELS).

*Contact author: abhishek.nag@ph.iitr.ac.in
†Contact author: j.fink@ifw-dresden.de
‡Contact author: agreco@fceia.unr.edu.ar
§Contact author: kejin.zhou@diamond.ac.uk

One of the fundamental bosonic excitations in metallic systems is plasmon, originating from collective charge-density oscillations in the presence of long-range Coulomb interactions [5]. Typically, in isotropic electron systems, the long-wavelength plasmon energy associated with the charge oscillations is finite. In layered three-dimensional (3D) electron systems, the 3D Coulomb interactions are poorly screened due to the confinement of charges to planes separated by dielectric blocks. Thus, although 3D Coulomb interactions tend to forbid gapless plasmons [6], for particular momenta perpendicular to the layers (q_z), charge oscillations that are out of phase may lead to formation of acoustic plasmons ($\omega \to 0$ as $q \to 0$) along with the gapped (optical) plasmons [7–10].

In layered systems like cuprates, optical plasmons were detected soon after the discovery of the high-T_C superconductivity using transmission-EELS (T-EELS) [11]. Acoustic-like plasmons in the cuprates, however, have only recently been observed with the development of the RIXS technique [12–17]. Due to the low energy of acoustic plasmons, their role has been discussed sparsely since the discovery of superconductivity [18–22]. More importantly, the cuprate superconductors, exhibiting anomalous electronic properties such as those observed in the pseudogap and the strange-metal phases [1,2], are widely studied for correlated electron physics. The observation of long-wavelength low-energy quantum fluctuations of charges along with spins [12,15,23–25] has, therefore, renewed efforts to develop a unified understanding of electron correlations, Coulomb and exchange interactions aiming toward a microscopic theory [26–29].

Correlation effects in cuprates lead to an enhancement of the quasiparticle electron mass. The mass enhancement factor can be denoted as m^*/m, where m^* and m are the band mass in the presence of interactions and that predicted by tight-binding calculations, respectively [30]. In contrast, a variety of descriptions can be found for the plasmon excitations in the cuprates. The dispersion of the optical plasmons observed using T-EELS has been described within mean-field random phase approximation (RPA) theories without explicitly considering electron correlations [31]. The dispersion of the acoustic-like plasmons observed using RIXS has been described using both free-electron layered models and models incorporating strong electron correlations such as the t-J-V model [12–15,28,29,32]. The charge carrier doping dependence of plasmon energies could not be explained within an RPA model, leading to the introduction of a scaling factor to the plasmon energies [12,13]. Recently, the t-J-V model in a large-N approximation was employed to explain the low-doping range dependence of plasmons [15,29]. A similar doping dependence was also discussed in Ref. [33], but only for the optical plasma frequency. In the strange metal phase, momentum-independent broad continua observed using reflection-EELS [34,35] have been described using holographic theories [36], while a RIXS study has found dispersive excitations in this phase [15]. This multitude of descriptions raises a pertinent question: Do electron correlations that affect the single-particle excitations strongly have any role to play in the collective charge excitations in cuprates, and what should be the appropriate framework used to describe it?

In this study, we provide a unified perspective on the importance of electron correlations on the dispersion of the acoustic-like plasmons in electron- and hole-doped cuprates probed by RIXS. We compare equal doping levels ($\delta = 0.16$) of archetypal hole-doped $La_{1.84}Sr_{0.16}CuO_4$ (LSCO), and electron-doped $La_{1.84}Ce_{0.16}CuO_4$ (LCCO). The similar lattice parameters of these systems enable investigation of the plasmons in the same momentum phase space. We observe dispersive coherent excitations for both O K- and Cu L_3-edge RIXS in both systems. For the equal doping level, we find that plasmon velocity in LSCO is smaller than that of LCCO, consistent with the former's smaller Fermi velocity derived from bare band electronic dispersion. However, within a free electron model, the plasmon velocities are overestimated when considering the bare Fermi velocities for both systems. We demonstrate that an appropriate fit to experimentally observed plasmon dispersion is possible within an RPA model with the inclusion of a system-dependent band renormalization parameter, and without which unrealistic values of dielectric constants and incoherent excitations are obtained. The acoustic-like plasmons can be accurately described by the t-J-V model, where bare band parameters provided as input get implicitly renormalized by electron correlations. Our findings reveal that plasmon dispersion in cuprates is affected by electron correlations like the single-particle excitations, and is accounted for by the band renormalization parameter in the RPA model. Thus, by comparing plasmon dispersions and bare band electron dispersion parameters, it is possible to assess the role and magnitude of electron correlations in different phases in the cuprates.

II. RESULTS

A. Electronic structure of LSCO and LCCO

Hole-doped LSCO and electron-doped LCCO belong to the family of single-layered cuprates, obtained upon doping parent systems La_2CuO_4. They crystallize in distinct structures, the K_2NiF_4-type T (LSCO) and Nd_2CuO_4-type T' (LCCO) [38]. In the T structure, O atoms form octahedral cages around Cu, while apical O atoms are absent in the Cu-O planes in the T' structure [see Fig. 1(a)], leading to different electronic ground states for the doped systems. A strong Cu-O hybridization and on-site Coulomb interactions give rise to the upper Hubbard band (UHB) and the Zhang-Rice singlet (ZRS) band in cuprates, as shown in Fig. 1(b) [37,39–46]. The electrostatic potential at the Cu sites is raised due to the lack of apical oxygen in LCCO compared to LSCO, resulting in a reduced charge-transfer energy (Δ_{CT}). Hole doping shifts the chemical potential (μ) to the ZRS, whereas electron doping shifts it to the bottom of the UHB. The charge carrier dynamics in these systems can therefore be investigated using x-ray spectroscopy by tuning the photon energy to resonant transitions to these bands. The x-ray absorption spectra (XAS) of LSCO and LCCO ($\delta = 0.16$), obtained at the Cu L_3- and O K-edge, respectively, are shown in Figs. 1(c) and 1(d). The Cu L_3-edge XAS peak corresponds to the transition to the UHB in both systems. In LSCO, the first peak in O K-edge XAS corresponds to the hole states, with the transition to the UHB occurring 1.5 eV higher [44,46,47]. In LCCO, the first peak in the O K-edge XAS is the transition to the UHB, lowered in energy due to the reduced Δ_{CT} and chemical shift of the

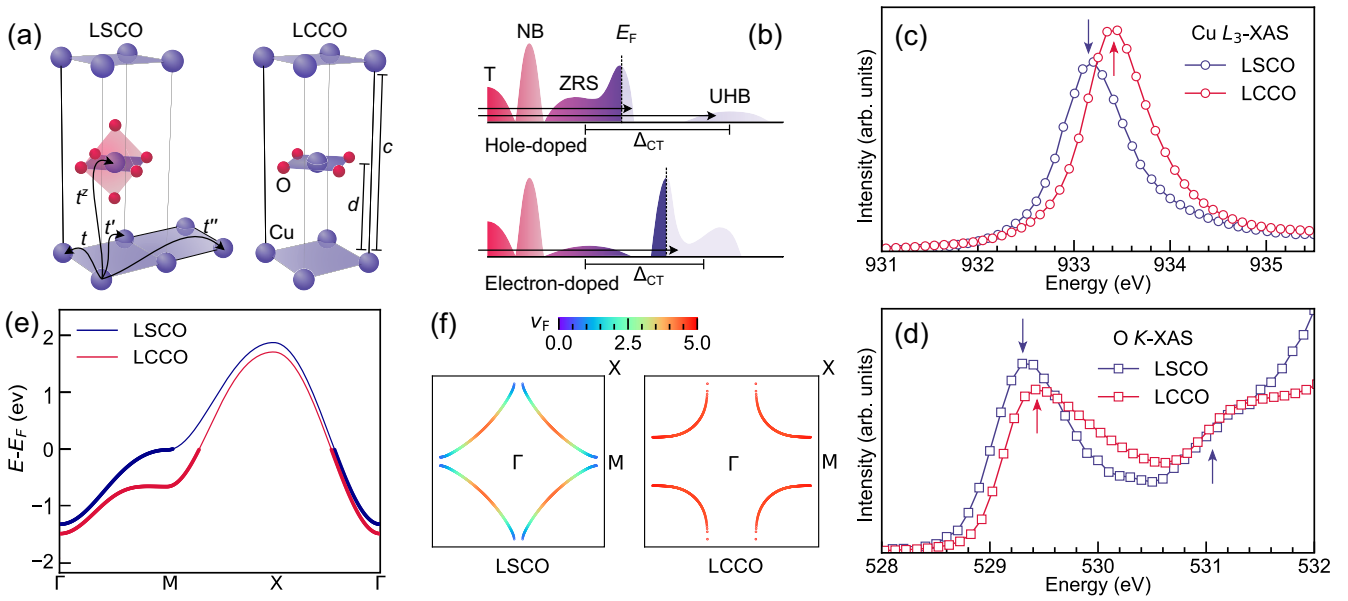

FIG. 1. Electronic structure of doped cuprates. (a) Schematic lattice structures of single-layered hole-doped LSCO and electron-doped LCCO showing the Cu-O planes and hopping pathways. O atoms are shown only around the central Cu atom. (b) Schematic representation of electron transitions within the multiband structure of hole- and electron-doped cuprates [37]. UHB, ZRS, NB, and T represent the upper Hubbard, Zhang-Rice singlet, nonbonding O, and the Zhang-Rice triplet bands, respectively. (c) Cu L_3-edge XAS of LSCO and LCCO. (d) O K-edge XAS of LSCO and LCCO ($\delta = 0.16$). Arrows mark the photon energies used to probe the plasmons. (e) One-band tight-binding electron dispersion of LSCO and LCCO [see Eq. (4) in Sec. V B]. (f) Fermi velocity distribution in LSCO and LCCO.

O 1s level, consistent with observations in electron-doped $Nd_{2-x}Ce_xCuO_4$ (NCCO) [46,47].

B. RIXS

Figures 2(a)–2(e) show the RIXS energy-momentum maps collected on LSCO and LCCO ($\delta = 0.16$) along the Cu-O in-plane direction h, with $k = 0.0$ and $l = 1.0$. We denote momentum transfers along h, k, and l directions in reciprocal lattice units, where $\mathbf{q} = (ha^*, kb^*, lc^*)$ ($a^* = 2\pi/a$, $b^* = 2\pi/b$, $c^* = 2\pi/c$, and $a = b$ and c are the in-plane and out-of-plane lattice parameters, respectively, see Table I). The incident photon energy for RIXS maps shown in Figs. 2(b) and 2(c) correspond to resonant transitions to the ZRS and the UHB at O K-edge in LSCO, respectively [see arrows in Fig. 1(d)]. The highly dispersive plasmon excitations are prominent at both incident energies. A hybridized nature of the doped charges in hole-doped cuprates was concluded based on a similar observation in $La_{1.88}Sr_{0.12}CuO_4$ recently [14]. Despite the Cu-O hybridized content of the ZRS and the UHB states, study at only the O K-edge is insufficient. In Fig. 2(a) we show the RIXS map at Cu L_3-edge for LSCO. We can identify faint spectral weight present which appears to follow the plasmon dispersion extracted from O K-edge RIXS on LSCO (shown by the blue dashed lines). Presence of these features is also evident in the momentum distribution curves shown in Fig. 2(f) for energy transfer between 0.225 and 0.515 eV. In contrast, our earlier investigation on LSCO and $Bi_2Sr_{1.6}La_{0.4}CuO_{6+\Delta}$ [32], along with studies on other hole-doped cuprates [23,48,49], did not reveal the presence of plasmons at the Cu L_3-edge. This is most likely because the plasmon spectral weight is expected to be the strongest at $l = 1.0$ [29], where we have investigated in this work. The presence of plasmons at the Cu L_3-edge, although extremely weak, validates their hybridized nature in the hole-doped cuprate. In LCCO, the dispersive plasmons are observed clearly for excitation at either the Cu L_3- or O K-edge, as shown in the RIXS maps in Figs. 2(d) and 2(e), respectively.

Representative fits to the plasmon excitations in the RIXS line profiles as described in Sec. V A are shown in Figs. 2(g)–2(j). The plasmon energies and widths extracted from the fits are presented in Fig. 3. It is clear from the similarity of plasmon energies and the widths that we probe the same

TABLE I. Parameters for LSCO and LCCO. In-plane lattice constant: a. Distance between the Cu-O layers: $d = c/2$. Doping concentration: δ. Superconducting transition temperature: T_c. Average bare Fermi velocity: $\langle v_F \rangle^{\text{bare}}$. Optical plasmon energy: Ω_p. Plasmon velocity obtained using $\langle v_F \rangle^{\text{bare}}$ in Eq. (1): v_p^{bare}. Experimental plasmon velocity: v_p^{RIXS}. Mass enhancement factor obtained using v_p^{RIXS} and renormalized $\langle v_F \rangle$ in Eq. (1): m^*/m.

	a (Å)	$d = c/2$ (Å)	δ	T_c (K)	$\langle v_F \rangle^{\text{bare}}$ (eVÅ)	Ω_p (eV)	v_p^{bare} (eVÅ)	v_p^{RIXS} (eVÅ)	m^*/m
LSCO	3.77	6.55	0.16	38	2.86	0.8 [51]	3.31	2.79	2.0
LCCO	4.01	6.23	0.16	7.87	4.58	1.2 [13]	4.94	4.20	1.7

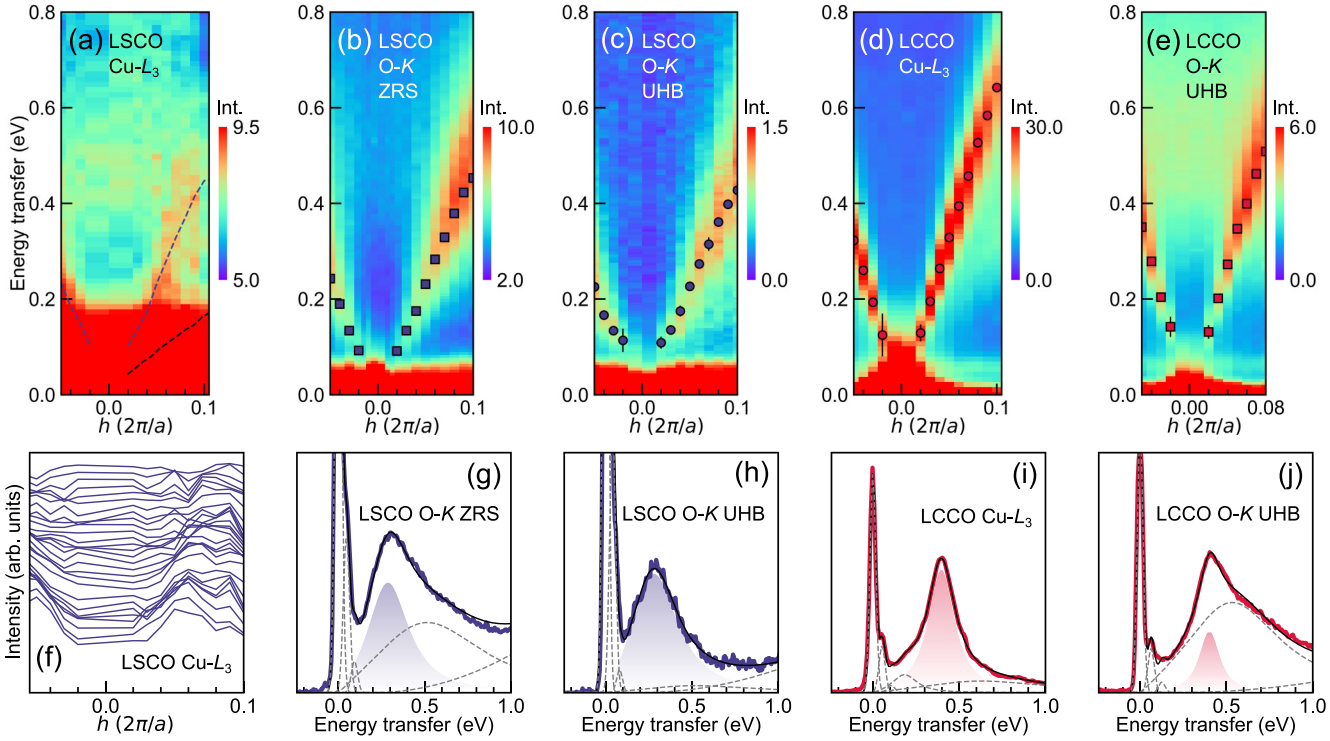

FIG. 2. Energy-momentum distribution of plasmons in LSCO and LCCO ($\delta = 0.16$). RIXS intensity maps with incident photon energy at (a) Cu L_3-edge, (b) O K-edge ZRS, and (c) O K-edge UHB, respectively, for LSCO. RIXS intensity maps with incident photon energy at (d) Cu L_3-edge and (e) O K-edge UHB, respectively, for LCCO. For all the data, $k = 0.0$ and $l = 1.0$. The color scales indicate scattered intensities in arbitrary units. The markers denote the extracted plasmon energies. In (a), the blue dashed line is the plasmon dispersion extracted from (b), and the black dashed line is the extended paramagnon dispersion from Ref. [25] for LSCO. (f) Momentum distribution curves for energy transfer between 0.225 and 0.515 eV for Cu L_3-edge RIXS on LSCO showing the plasmons. (g)–(j) RIXS line spectra from (b)–(e) at $h = 0.06$. The dashed lines are elastic, lattice, magnetic, and background components as described in Sec. V A. The shaded distributions are the fitted plasmon peaks which can be compared with the calculated charge susceptibility line profiles in Figs. 4(f)–4(h).

charge oscillations at Cu L_3- and O K-edges for LCCO, and the ZRS and UHB peak at O K-edge for LSCO [Fig. 3(a)]. The plasmons exhibit a nearly linear dispersion for small h values; however, since we cannot resolve the plasmon peaks below $h = 0.02$, and a gap may exist at $h, k = 0.0$ due to interlayer hopping (t_z) [28,50], we describe these excitations to be acoustic-like. Note that an upper limit of t_z was estimated to be 7 meV for LSCO and LCCO [32,50], which is negligibly small to influence the analysis presented in this work. We observe that the plasmon energies for LSCO are smaller than LCCO for the same doping level and at the same $h, k = 0.0, l = 1.0$ values. The plasmons in LSCO are more damped than LCCO, as can be seen from Fig. 3(b), where the extracted damping factor (γ/ω_0) is plotted. γ and ω_0 represent the plasmon width (damping $\sim$ inverse lifetime) and plasmon pole energy, respectively. γ/ω_0 is found to be less than 1 in the probed momentum phase space, signifying the coherence of the plasmons.

C. Effective masses and Fermi velocities in LSCO and LCCO

For the same amount of electron- and hole doping, the plasmon energies extracted from RIXS for LSCO are smaller than in LCCO [Fig. 3(a)], with plasmon velocities $v_p^{\mathrm{LSCO}} = 2.79 \pm 0.04$ eVÅ and $v_p^{\mathrm{LCCO}} = 4.20 \pm 0.01$ eVÅ. We first attempt to qualitatively describe the observed plasmon dispersion using the homogenous free-electron layered model, or Fetter-Apostol model [see Eq. (12)] [7,8]. Note that this free-electron model is in the hydrodynamic limit [7] or in RPA [8], and also does not consider interlayer hopping, and as such is not strictly applicable to the cuprates. Although less rigorous compared to many-body models, its simple analytic form allows a rudimentary association of the electronic band parameters to the acoustic plasmon dispersion and the optical plasmon frequency Ω_p. The acoustic plasmon velocity v_p at $l = 1.0$ and small in-plane momentum can be related to the average Fermi velocity $\langle v_F \rangle$ using Eq. (12) by

$$v_p = \sqrt{\frac{\langle v_F \rangle^2}{2} + \frac{d^2\Omega_p^2}{4}}, \tag{1}$$

where d is the distance between planes. Assuming that the plasmons are unaffected by electron correlations, we can then use experimentally reported Ω_p (see Table I) and bare $\langle v_F \rangle$ extracted from electron band dispersion to approximately estimate the v_p. We take tight-binding derived bare parameters for LSCO and NCCO (for LCCO) from Ref. [52] [see Eq. (4) in Sec. V B], and compute the chemical potential μ for doping $\delta = 0.16$. In Fig. 1(e) we show the bare band dispersion for LSCO and LCCO. The $3d$ band is close to half-filling for hole-doped cuprates, while for electron-doped cuprates the band filling is about 70%. Due to the proximity to the van

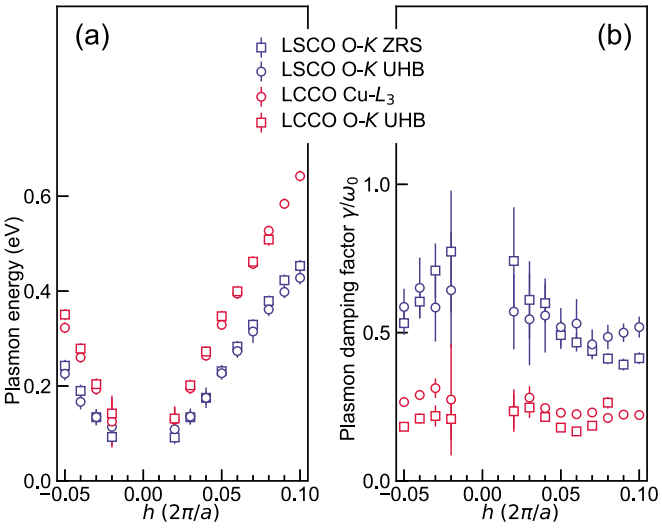

FIG. 3. Plasmon energies and lifetimes in LSCO and LCCO ($\delta = 0.16$). (a) Plasmon energies extracted from fits to RIXS spectra at O K-edge ZRS and O K-edge UHB for LSCO and Cu L_3-edge and O K-edge UHB for LCCO. (b) Plasmon damping factor (γ/ω_0) extracted from the same fits.

Hove filling, this results in a smaller average bare Fermi velocity $\langle v_F\rangle^{\mathrm{LSCO,bare}} = 2.86\,\mathrm{eV\AA}$ than $\langle v_F\rangle^{\mathrm{LCCO,bare}} = 4.58\,\mathrm{eV\AA}$ [shown in Fig. 1(f)]. Using these values in Eq. (1), we obtain $v_p^{\mathrm{LSCO,bare}} = 3.31\,\mathrm{eV\AA}$ and $v_p^{\mathrm{LCCO,bare}} = 4.94\,\mathrm{eV\AA}$. It is expected that the plasmon velocities in hole-doped cuprates are smaller than the electron-doped cuprates with similar d, due to smaller $\langle v_F\rangle$; however, as shown in Fig. 4(a), the Fetter model with the bare band parameters overestimates the plasmon velocities by 17% compared to the values extracted from RIXS (see Table I). Conversely, if we use Eq. (1) and v_p's extracted from RIXS, we obtain $\langle v_F\rangle^{\mathrm{LSCO}} = 1.36\,\mathrm{eV\AA}$ and $\langle v_F\rangle^{\mathrm{LCCO}} = 2.71\,\mathrm{eV\AA}$. These values are nearly 50% of the bare band estimates for both systems. Therefore, to explain the experimental results in this approximate model, one needs to use renormalized band dispersions which amount to mass enhancement of $m^*/m = 2.0$ and $m^*/m = 1.7$ for LSCO and LCCO, respectively.

D. Random phase approximation

Next, we consider the explicit description of the plasmons within an RPA framework with long-range Coulomb interaction for a layered lattice system (see Sec. V B for details

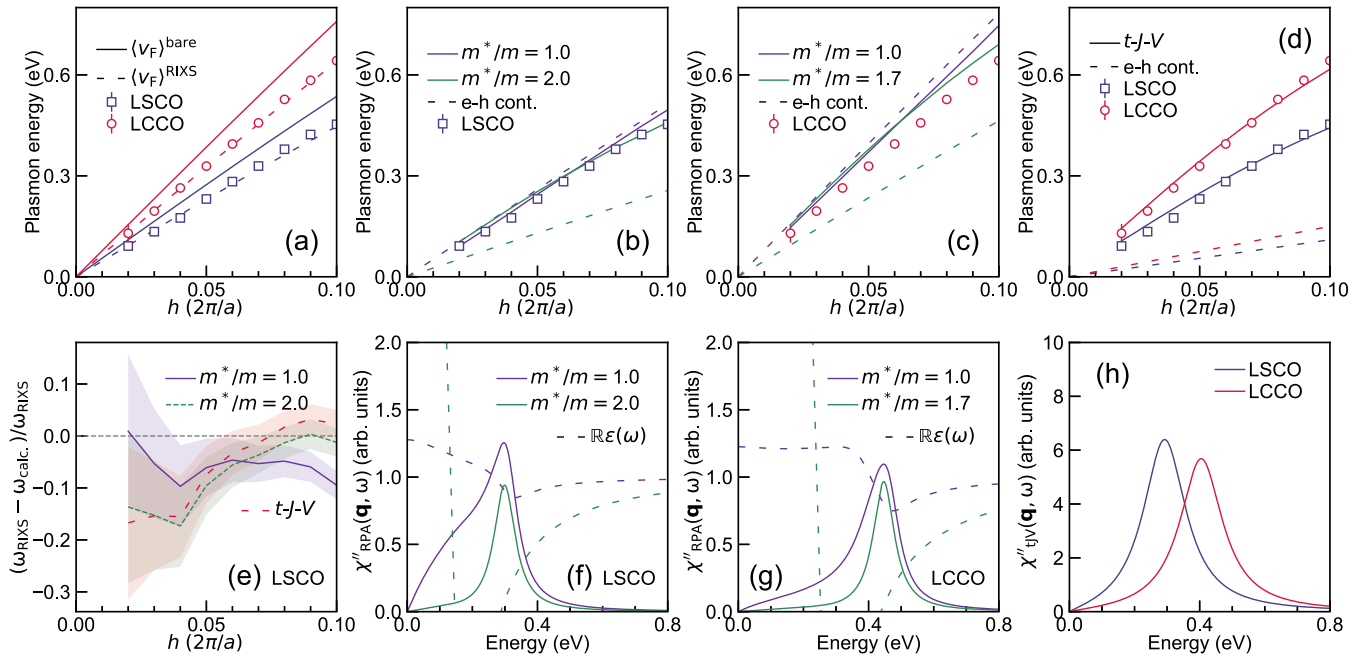

FIG. 4. Comparison of plasmons to weak- and strong-electron coupling models. (a) Plasmon energies from RIXS for LSCO and LCCO (markers). Lines are plasmon energies calculated using the free-electron Fetter-Apostol model [Eq. (1)] and different $\langle v_F\rangle$s for LSCO and LCCO. (b) Plasmon energies from RIXS for LSCO (markers). Lines are plasmon energies (continuous) and upper boundaries of electron-hole continua (dashed) calculated using the weak-coupling RPA model with different m^*/m values for LSCO. (c) Same as in (b) for LCCO. (d) Plasmon energies from RIXS for LSCO and LCCO (markers). Lines are plasmon energies (continuous) and upper boundaries of electron-hole continua (dashed) calculated using the strong-coupling t-J-V model and bare band parameters for LSCO and LCCO. (e) Momentum-dependent deviation of the plasmon energies calculated using the RPA and the t-J-V models from experiments on LSCO. The shaded areas represent the propagated fitting errors from RIXS spectra. (f) Charge susceptibilities (continuous lines) and real part of the dielectric functions (dashed lines) at $h = 0.06$ obtained from the RPA model with different m^*/m values for LSCO. (g) Same as in (f) for LCCO. (h) Charge susceptibilities obtained from the t-J-V model at $h = 0.06$ for LSCO and LCCO. The charge susceptibility line profiles in (f)–(h) can be compared to corresponding plasmon peaks in RIXS [Figs. 2(g)–2(j)]

TABLE II. Parameters extracted by fitting experimental plasmon dispersions to the different models.

	Model	m^*/m	V_c (eV)	α	$\epsilon_\parallel/\epsilon_0$	$\epsilon_\perp/\epsilon_0$
LSCO	RPA	1.0	0.49	0.5	14.1	85.1
	RPA	2.0	7.6	3.7	6.72	5.49
	t-*J*-*V*	-	18.8	4.1	3.01	2.22
LCCO	RPA	1.0	0.9	0.6	10.1	40.8
	RPA	1.7	9.2	3.2	5.05	3.81
	t-*J*-*V*	-	30.0	3.5	1.71	1.17

of the implementation). Note that we have ensured that the calculations are consistent with the experimentally reported values of Ω_p for both systems. In Figs. 4(b) and 4(c), we show the plasmon dispersion extracted from plasmon peaks in $\chi''_{\rm RPA}(\mathbf{q},\omega)$ calculated with bare and renormalized band parameters so that $m^*/m = 1.0$ and $m^*/m = 2.0$ for LSCO, and $m^*/m = 1.0$ and $m^*/m = 1.7$ for LCCO. Also plotted are the upper boundaries of the electron-hole continua for the respective m^*/m values. For both systems, in the long-wavelength limit, the agreement with the experimental results appears to be slightly better for $m^*/m = 1.0$, while above $h = 0.06$, the calculated results for $m^*/m > 1.0$ have smaller deviations from experiments. The momentum-dependent deviation from the experimental plasmon energies for LSCO is highlighted in Fig. 4(e), showing the better agreement with $m^*/m > 1.0$ for larger momenta and energies. It should also be noted from Figs. 4(b) and 4(c) that for $m^*/m = 1.0$, the plasmons are within the continuum boundary, while for $m^*/m > 1.0$, they are clearly above the continuum. Figures 4(f) and 4(g) show the $\chi''_{\rm RPA}(\mathbf{q},\omega)$ and the real part of the dielectric function $\mathbb{R}\epsilon(\omega)$ for $h = 0.06$, which undergoes a sign change only for $m^*/m > 1.0$. This signifies that true plasmon resonances which are long-lived are obtained only for $m^*/m > 1.0$. We can compare this observation to the experimentally extracted ratio γ/ω_0 [see Fig. 3(b)]. The γ/ω_0 values are less than 1, which means that experimentally we observe the plasmons as coherently propagating excitations. Additionally, the ratio of in-plane to out-of-plane dielectric constants obtained from the RPA analysis (see Table II in Sec. V B) for $m^*/m > 1.0$ is 1.22 for LSCO and 1.32 for LCCO, while for $m^*/m = 1.0$ the respective ratios are unrealistic ($\ll 1$): 1/6 and 1/4. Thus, the layered lattice RPA model also suggests the use of renormalized band parameters for both systems for describing the plasmons.

E. *t*-*J*-*V* model

In this section, we model the observed plasmon dispersion with the *t*-*J*-*V* model with long-range Coulomb interaction in a large-N approximation for a layered lattice system, where our inputs are the bare band parameters (see Sec. V B for details of the implementation). Once again, we have verified that the calculations are consistent with the experimentally reported values of Ω_p for both systems. In Fig. 4(d), we show that there is a good agreement between the plasmon dispersions obtained experimentally and those extracted from plasmon peaks in the calculated $\chi''_{\rm tJV}(\mathbf{q},\omega)$. The plasmons appear as well-defined peaks [Fig. 4(h)] and above the electron-hole continuum. This is because the bare band parameters are implicitly renormalized by electron correlations within the theory. To have an estimation of the band renormalization one can see Eq. (25) in Sec. V B 4, which gives m^*/m of around 4.5 for both systems. Also, the ratio of the in-plane to out-of-plane dielectric constants obtained from the *t*-*J*-*V* analysis is found to be 1.35 for LSCO and 1.46 for LCCO (see Table II in Sec. V B). Thus, the strongly correlated electron model also describes the plasmons appropriately, without explicitly invoking renormalized band parameters.

III. DISCUSSION

A. Plasmon dispersion and correlations

Despite the large diversity in material-dependent properties, the correlated electron nature of cuprates is widely acknowledged. While the single-particle electron excitations in cuprates clearly show the effects of correlations like mass enhancement and incoherence, charge excitations like plasmons have been described using theories ranging from free electron to weak- and strong coupling. The optical plasmon energy Ω_p for zero momentum in the mean-field RPA of homogeneous layered electron systems is proportional to $\sqrt{1/m^*}$ [53,54]. The optical plasmon dispersion up to second order in q in this model is $\Omega_p + Aq^2$, where A is a dispersion coefficient dependent on m^*. Even so, the optical plasmon dispersion observed in $Bi_2Sr_2CaCu_2O_8$ using T-EELS could be described using the bare band parameters [53,54]. Notably, in Sr_2RuO_4, a system for which ARPES estimated $m^*/m \approx 4$, optical plasmons observed using T-EELS have been modeled using bare band parameters [55,56]. This was explained on the basis of optical spectroscopy data [57] which found an energy-dependent m^*/m: close to 4 below 0.2 eV and close to 1 at higher energies. Resilient quasiparticles at high energies have been predicted by density-functional theory extended by dynamical mean-field theory calculations [58], and it appears that in Sr_2RuO_4 the high-energy plasmons of 1.5 eV are unaffected by correlations.

Our observations extend this discussion by focusing on the low-energy acoustic-like plasmon dispersion in LSCO and LCCO, in which the situation seems to be different from the aforementioned. We observe that the plasmon velocity of LSCO is approximately 1.5 times smaller than LCCO for a doping $\delta = 0.16$. Since the plasmons are collective excitations involving electrons near the Fermi surface, one can qualitatively explain this observation by considering the 1.5 times smaller $\langle v_F \rangle$ in the hole-doped cuprate. However, when using the $\langle v_F \rangle$s derived from bare bands, the plasmon energies are overestimated for both systems in the free electron model. Thus, for cuprates it seems that the acoustic-like plasmons cannot be described using bare band parameters and it is necessary to consider the effects of correlation for a quantitative analysis. Within the RPA approach, the agreement of the dispersion with $m^*/m = 1$ worsens as q increases, while it improves for $m^*/m > 1$. Although it may seem that the effects of correlation may be fully relaxed in the long-wavelength limit, using the $m^*/m = 1$ band parameters results in plasmons appearing within the electron-hole continuum and unreasonable dielectric constant values for either system

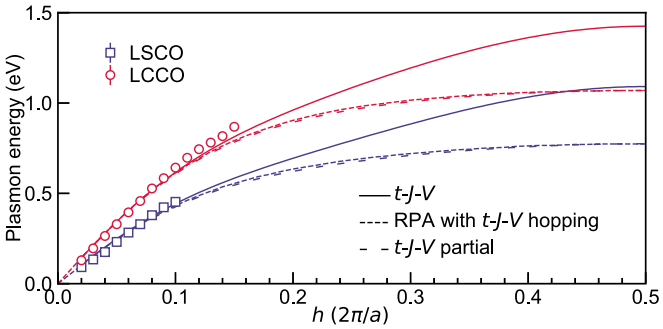

FIG. 5. Momentum dependence of correlation effects on plasmons. Plasmon energies from RIXS for LSCO and LCCO (markers). Continuous lines are plasmon energies calculated using the full t-J-V model. Dense dashed lines are plasmon energies calculated using the RPA model with renormalized band parameters obtained from the t-J-V model. The match between the two models at long wavelengths suggest that RPA with the renormalized band mass formalism accounts for the effects of electron correlations in this region of momentum space. Locally strong correlation effects stemming from double occupancy prohibition that are absent in RPA lead to deviations only at large momenta. Sparse dashed lines are plasmon energies calculated using a partial t-J-V model (see Sec. V B 4). The overlapping dispersions obtained from the RPA and the partial t-J-V model show that despite the apparent complication of the t-J-V formalism with respect to RPA, it has a "hidden" RPA structure including the effects of the electronic correlations.

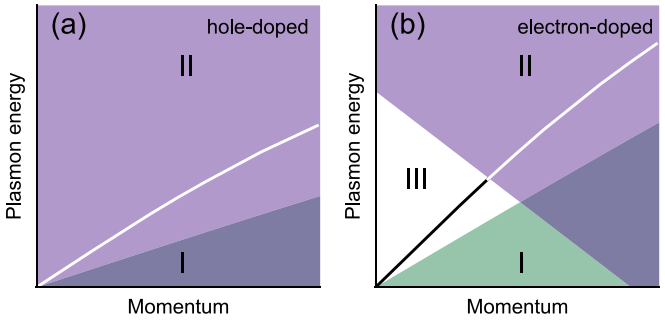

FIG. 6. Broadening of plasmons due to a decay into single-particle excitation continua. The electron-hole continuum due to intraband transitions (I). The continuum due to Umklapp scattering related to interband transitions (II). Energy-momentum pocket devoid of continuum in electron-doped systems (III). White lines: Plasmon damping caused by decay into the continuum from single-particle excitations. (a) LSCO, close to half-filled conduction band. (b) LCCO with additional filling of the conduction band, causing a pocket in the continuum of the interband continuum.

in our model. The value of the mass enhancement factor $m^*/m = 2.0$ for LSCO is numerically equal to that measured using ARPES at the nodal point [59]. However, this match should not be overemphasised, given that the result from the plasmons represents an average effect over the entire Brillouin zone (BZ), which means including the antinodal region near the saddle point $(\pi, 0)$ with a low v_F, and the nodal region near $(\pi, \pi)/2$. Also, smaller m^*/m values are observed in the RPA models for LCCO than LSCO. Although weaker correlations are expected in electron-doped than in hole-doped cuprates [38,39,60–65], it should be noted that the value of m^*/m for LCCO was obtained using the band parameters of NCCO in the calculations. This is due to unavailability of the band parameters for LCCO.

It can be seen from Fig. 4(e) that the deviation from the experiments in the t-J-V model, in which the correlation effects are implicit, is similar to that obtained from RPA for $m^*/m > 1$ [smaller (larger) difference at high (low) q]. In the t-J-V model, the bare band parameters get renormalized by the doping δ and J, and additionally the charge response contains fluctuations of the constraint that prohibit double occupancy at a given site. To compare with the RPA model, we use the renormalized band parameters obtained from t-J-V in the RPA and plot the calculated plasmon dispersions for LSCO and LCCO in Fig. 5. We observe that in the long-wavelength region, the t-J-V and RPA plasmon dispersions coincide. However, at short wavelengths, the RPA plasmon dispersions deviate from the t-J-V. In Fig. 5, we also plot plasmon dispersions obtained from the t-J-V excluding some bosonic self-energy components which carry information of the coupling between charge fluctuations and fluctuations of the Lagrange multiplier that force the non double occupancy constraint (see Sec. V B 4). Exclusion of these components from the t-J-V model results in a mathematically identical form of charge susceptibility to RPA, and hence identical plasmon dispersions are obtained for the two models. Thus, it is evident that the use of renormalized band parameters, i.e., the inclusion of m^*, in RPA accounts for electron correlations through the enhanced band mass at long wavelengths, while the locally strong correlation effects stemming from double occupancy prohibition that are absent in RPA lead to deviations only at large momenta. It would be interesting to probe the acoustic-like plasmons till large momenta to (a) fit the long-wavelength acoustic-like plasmon dispersion using RPA with the inclusion of an effective mass m^* and using the t-J-V model, and (b) evaluate the nature of the predicted disagreement between RPA and the t-J-V model at large momenta ($h > 0.25$).

B. Plasmon width

In a free-electron model there is no momentum phase space for the decay of an acoustic or an optical plasmon into intraband electron-hole excitations (Landau damping) if the plasmon is above the continuum (region I in Fig. 6). Moreover, in the long-wavelength region, the plasmon should be undamped. Nevertheless, non-resolution-limited plasmons are observed in experiments. For finite q a q^2 dependence was predicted due to a decay into electron-hole pair excitations, but the theoretical estimates of the broadening were an order of magnitude smaller than the experimentally determined values [66]. Calculations for decay via phonon and impurity-assisted intraband transitions were also found to be insufficient [67,68]. Thus, the plasmon width had been a puzzle for long time. Finally, it was theoretically proposed [69] that plasmon width appears through a decay into the continuum formed due to interband excitations (region II in Fig. 6). The latter originate from Umklapp processes due to the square of the Fourier transform of the pseudopotential of the ions in neighboring BZs. Experimentally, this was

supported by EELS on alkali metals, where the plasmon width was found to be proportional to the square of the pseudopotential [70,71]. From the $\gamma/\omega_0 < 1$ values extracted from RIXS [Fig. 3(b)], we can see that the damping of acoustic plasmons in LSCO is twice as large as LCCO. In the case of a half-filled band such as in LSCO and a k_F equal to half of the BZ, the interband continuum extends to $(q, \omega = 0)$. Thus, the acoustic plasmons are damped additionally regardless of the intraband continuum. Upon changing the band filling, a pocket appears in the interband continuum in the low-energy low-momentum region [region III in Fig. 6(b)]. In this case (e.g., in LCCO), the acoustic plasmon will be less damped. Here, we mention that such pockets causing nearly undamped plasmons at low energy were previously described in T-EELS studies of K-doped graphite [72]. In Ref. [73] the authors considered the Hubbard model in the presence of the long-range Coulomb interaction using dynamical mean-field theory, and plasmons were obtained if one-particle self-energy effects and vertex corrections due to correlations are treated properly. The inclusion of electronic self-energy effects leads to a broadening of the plasmons (along with mass enhancement), and an energy dependence of the mass enhancement cannot be ruled out [57,74,75]. One-particle self-energy effects can be expected from the interaction between carriers and the rich variety of low-energy charge excitations in the energy scale of J [76–78], which may lead to further differences in the plasmon lifetimes of LSCO and LCCO. Further contribution to the broadening of the plasmons may appear from plasmon-phonon decays. Instead of material-specific tuning of the broadening, in our calculations we have considered a minimal momentum- and energy-independent broadening $\Gamma = 0.04\,\text{eV}$ $(0.1t)$ comparable to experimental energy resolution to study the plasmon behavior. It should be noted that our analysis is performed in the context of the t-J-V model, i.e., the t-J model, which can be derived from the Hubbard model in the large-U limit, in the presence of the long-range Coulomb interaction. Presence of plasmons in our calculations in spite of the strong correlations shows the consistency of our results with those of Ref. [73].

IV. CONCLUSIONS

We have investigated LSCO and LCCO at equal doping using RIXS, and have observed acoustic-like plasmons having different velocities. We find that the plasmon parameters (energy and lifetime) are identical for a given system irrespective of the probed site (Cu or O). While the RIXS cross section is typically dominated by local-site effects, this observation highlights that the probed charge excitations are nonlocal and site independent, similar to magnetic excitations, due to the hybridized nature of valence charge fluctuations. We show that to appropriately describe the acoustic-like plasmon dispersions in cuprates in a mean-field RPA approach, one has to consider renormalized band dispersion parameters. A similar renormalization of the bare band parameters occurs implicitly in the strong-coupling t-J-V model. This holds true for both sides of the cuprate doping phase diagram, where we observe $m^*/m > 1$ for both LSCO and LCCO. The comparison with the t-J-V model justifies the use of the renormalized band parameters in the RPA approach to effectively represent the mass enhancement stemming from electron correlations at long wavelengths. Therefore, the weak-coupling nature of the RPA should not be used to dismiss its practical usage in cuprates without due consideration. The role of correlations in the two-particle charge response extends beyond a simple adjustment of band parameters. An enhanced band mass reduces the average Fermi velocity and pushes the electron-hole continuum below the plasmon energies, allowing the observation of plasmons as resonant collective excitations. Even though here we have used a uniform mass enhancement contribution to the acoustic-like plasmon dispersion, optical and ARPES studies on Sr_2RuO_4 have suggested the mass enhancement factors to be dependent on the quasiparticle energy [57,74]. Typically the spin exchange energies ($\sim$0.2 eV) are much smaller than the optical plasmon energies of about 1 eV. This may rationalize the non-dependence of optical plasmon dispersion on electron correlations observed using T-EELS in cuprates and ruthenates [31,55,56,79], in contrast to the acoustic plasmons. The difference in the influence of electron correlations on acoustic and optical plasmons will be the subject of our research in the near future.

V. METHODS

A. Experimental details

A single crystal of $La_{1.84}Sr_{0.16}CuO_4$ (LSCO) grown by the floating-zone method and used for a previous report on plasmons [32] was reused for this experiment. The crystal was re-cleaved before measurement at each edge, in vacuum. Hole doping of $\delta = 0.16$ was verified using magnetization measurements of LSCO corresponding to a superconducting transition temperature of 38 K.

High-quality $La_{2-x}Ce_xCuO_4$ films were grown on $SrTiO_3$ substrates via the pulsed laser deposition technique with 100 nm thickness. The films have a linearly varying Ce concentration ($x = 0.1$ to 0.19) along the surface of the substrate, fabricated by the continuous moving mask technique [80]. The direction of varying concentration is aligned normal to the RIXS scattering plane. The c-axis lattice constants and superconducting transition temperatures measured along the concentration gradient direction are consistent with results from single-doping LCCO films [81]. For $x = 0.16$, a superconducting transition temperature of 7.87 K was observed using resistivity measurements.

The pressure inside the sample vessel was maintained around 5×10^{-10} mbar. The samples were cooled down to 25 K. While this means that the LSCO was below and the LCCO was above T_C, a recent article [15] did not find significant change in the plasmon dispersion in this temperature range. The XAS were collected as total electron yield in normal incidence geometry with σ polarization, so that the electric field was in the Cu-O plane. High-energy-resolution RIXS spectra were collected at Cu L_3-($\Delta E \simeq 0.045\,\text{eV}$) and O K- ($\Delta E \simeq 0.043\,\text{eV}$) edges with σ polarization at the I21-RIXS beamline, Diamond Light Source, United Kingdom [82]. The zero-energy transfer position and energy resolution were determined from subsequent measurements of elastic peaks from an adjacent carbon tape. Negative and positive

values of h represent the grazing-incident and grazing-exit geometries, respectively.

RIXS data were normalized to the incident photon flux, and subsequently corrected for self-absorption effects prior to fitting. A Gaussian line shape with the experimental energy resolution was used to fit the elastic line. Gaussian line shapes were also used to fit the low-energy phonon excitations at ∼0.045 eV and their overtones. The scattering intensities $S(\mathbf{q}, \omega)$ of the plasmons, bimagnons, and paramagnons, dependent on the imaginary part of their respective dynamic susceptibilities $\chi''(\mathbf{q}, \omega)$, were modeled as

$$S(\mathbf{q}, \omega) \propto \frac{\chi''(\mathbf{q}, \omega)}{1 - e^{-\hbar\omega/k_B T}}, \tag{2}$$

where k_B, T, and $\hbar$ are the Boltzmann constant, temperature, and the reduced Planck constant. A generic damped harmonic oscillator model was used for the response function

$$\chi''(\mathbf{q}, \omega) \propto \frac{\gamma\omega}{\left[\omega^2 - \omega_0^2\right]^2 + 4\omega^2\gamma^2}, \tag{3}$$

where ω_0 and γ are the undamped frequency and the damping, respectively.

First, we extracted the zone-centre energy, amplitude, and width of the broad incoherent mode at $h = 0.01$ and, concluding this to be a bimagnon, fixed its amplitude and width for the whole momentum range [32]. The energy values of the bimagnons were allowed to vary within ±20 meV. An additional paramagnon component was added for the RIXS spectra at the Cu L_3-edge for LCCO. Significant correlations were found below $h < 0.02$, between the elastic, phonon, and plasmon amplitudes and energies, and hence the plasmon energy values determined in these regions are less conclusive and not reported. A high-energy quadratic background was also included in the fitting model to account for the tailing contribution from dd excitations above 1.5 eV. Representative fits using this model are shown in Figs. 2(g)–2(j).

B. Theory details

1. Band dispersion and Coulomb repulsion

Based on *ab initio* calculations, the electron band dispersion for the cuprates was proposed as

$$E_{\mathbf{k}} = E_{\mathbf{k}}^{\parallel} + E_{\mathbf{k}}^{\perp}, \tag{4}$$

where the in-plane dispersion $E_{\mathbf{k}}^{\parallel}$ (Ref. [52]) and the out-of-plane dispersion $E_{\mathbf{k}}^{\perp}$ are given, respectively, by

$$E_{\mathbf{k}}^{\parallel} = -2t(\cos k_x + \cos k_y) - 4t' \cos k_x \cos k_y - 2t''(\cos 2k_x + \cos 2k_y) - \mu, \tag{5}$$

$$E_{\mathbf{k}}^{\perp} = -\frac{t_z}{4}(\cos k_x - \cos k_y)^2 \cos k_z\,, \tag{6}$$

with μ as the chemical potential. The different hopping pathways in the materials are shown in Fig. 1(a). We use the bare parameters [52]: $t = 0.4$ eV, $t'/t = -0.09$, and $t''/t = 0.07$ for LSCO, and $t = 0.4$ eV, $t'/t = -0.24$, and $t''/t = 0.15$ for LCCO. The parameters used for LCCO are those given in Ref. [52] for NCCO, due to unavailability of data for LCCO. In the out-of-plane dispersion $E_{\mathbf{k}}^{\perp}$ we have replaced $\cos k_z$ with 1 in the calculation, i.e., the contribution of $E_{\mathbf{k}}^{\perp}$ is independent of k_z, which leads to a vanishing plasmon gap at the zone center, even for a finite value of t_z. This is justified by the fact that the plasmon gap in LSCO and LCCO, if it exists, is small and at present inaccessible experimentally, a topic which was discussed in depth in Ref. [50]. In other words, the presence of $\cos k_z$, as it was in Refs. [15,32,50], and the $E_{\mathbf{k}}^{\perp}$ dispersion is nearly irrelevant to the present analysis. Without losing generality, we have assumed $t_z/t = 0.01$ for both systems. We have also neglected t''' and t_z'. Finally, we compute the chemical potential μ for each case for doping $\delta = 0.16$, which gave $\mu = -0.24$ eV and $\mu = 0.038$ eV for LSCO and LCCO, respectively.

Earlier works [7,10,83] considered the long-range Coulomb interaction $V(\mathbf{q})$ for homogeneous layered electron gas as

$$V(\mathbf{q}) = V(q_{||}, q_z) = \frac{q_{||}d}{2} \frac{\sinh(q_{||}d)}{\cosh(q_{||}d) - \cos(q_z d)}. \tag{7}$$

Here, we use the long-range Coulomb interaction $V(\mathbf{q})$ for a layered lattice system for the RPA and t-J-V models:

$$V(\mathbf{q}) = \frac{V_c}{A(q_x, q_y) - \cos q_z}, \tag{8}$$

where $V_c = e^2 d(2\epsilon_\perp a^2)^{-1}$ and

$$A(q_x, q_y) = \alpha(2 - \cos q_x - \cos q_y) + 1. \tag{9}$$

These expressions are easily obtained by solving Poisson's equation on the lattice [84]. Here, $\alpha = \tilde{\epsilon}/[(a/d)^2]$, $\tilde{\epsilon} = \epsilon_\parallel/\epsilon_\perp$, and $\epsilon_\parallel$ and $\epsilon_\perp$ are the dielectric constants parallel and perpendicular to the planes, respectively. It is important to note that in the present $V(\mathbf{q})$ model we have two dielectric constants instead of one as in Refs. [7,10]. e is the electric charge of electrons; a is the in-plane lattice constant and the in-plane momentum $\mathbf{q}_\parallel = (q_x, q_y)$ is calculated in units of a^{-1}; similarly, d is the distance between the Cu-O planes, and the out-of-plane momentum q_z is calculated in units of d^{-1}. In the present work, we consider V_c and α as independent parameters, and from them we can estimate $\epsilon_\parallel$ and $\epsilon_\perp$ and discuss their reliability.

2. Random phase approximation

In RPA the charge correlation function is given by the well-known expression [85]

$$\chi_{\mathrm{RPA}}(\mathbf{q}, i\omega_n) = \frac{\chi^{(0)}(\mathbf{q}, i\omega_n)}{1 - V(\mathbf{q})\chi^{(0)}(\mathbf{q}, i\omega_n)}, \tag{10}$$

where $\chi^{(0)}(\mathbf{q}, i\omega_n)$ is the usual Lindhard function,

$$\chi^{(0)}(\mathbf{q}, i\omega_n) = \frac{2}{N_s} \sum_{\mathbf{k}} \frac{n_F(E_{\mathbf{k}-\mathbf{q}}) - n_F(E_{\mathbf{k}})}{i\omega_n - E_{\mathbf{k}} + E_{\mathbf{k}-\mathbf{q}}}, \tag{11}$$

which accounts for the particle-hole continuum. $\mathbf{q}$ is a three-dimensional wave vector, ω_n is a boson Matsubara frequency, and the factor 2 comes from the spin summation. N_s is the number of sites in each plane and n_F is the Fermi distribution. The denominator in Eq. (10) is the RPA dielectric function $\varepsilon(\mathbf{q}, i\omega_n) = 1 - V(\mathbf{q})\chi^{(0)}(\mathbf{q}, i\omega_n)$.

After performing the analytical continuation $i\omega_n \to \omega + i\Gamma$ in $\chi_{\mathrm{RPA}}(\mathbf{q}, i\omega_n)$, we obtain the imaginary part of the charge-charge correlation functions $\chi''_{\mathrm{RPA}}(\mathbf{q}, \omega)$, which can be directly

compared with RIXS. Γ influences the width of the plasmon, and its effect on the plasmon peak position is strongest when it becomes comparable to undamped plasmon energy (overdamped condition). From Fig. 3(b), we see that this condition may be applicable only close to the zone center. As discussed in the main text, several factors can affect the plasmon width. Here, we consider a minimal momentum- and energy-independent broadening $\Gamma = 0.04\,\text{eV}$ $(0.1t)$ comparable to experimental energy resolution to study the plasmon behavior [29,33,50,86]. The RPA calculation is a weak coupling approach and, in principle, the electron dispersion $E_{\mathbf{k}}$ [Eq. (4)] is given by the bare band [52]. However, as discussed in the text, the electron hopping parameters t, t', and t'' are renormalized to account for $m^*/m > 1$.

The analytical relation between plasmon and Fermi velocities [Eq. (1)] in the homogeneous free-electron layered model by Fetter-Apostol [7,8] is derived from the plasmon energy:

$$\omega_{\text{p}} = \sqrt{\frac{\langle v_{\text{F}}\rangle^2}{2} q_{\parallel}^2 + \Omega_{\text{p}}^2 \frac{q_{\parallel} d}{2} \frac{\sinh(q_{\parallel} d)}{\cosh(q_{\parallel} d) - \cos(q_{\perp} d)}}, \tag{12}$$

obtained by using the Coulomb potential in Eq. (7) and the denominator in Eq. (10) [7]. Note that in the negligible conduction dissipation limit, the factor $\langle v_{\text{F}}\rangle^2 q_{\parallel}^2/2$ is absent (for $\omega_{\text{p}}^2 \gg \langle v_{\text{F}}\rangle^2 q_{\parallel}^2/2$) [87]. This is not the case for the energy-momentum range of plasmons probed in this work.

3. *The layered* t-J-V *model and the large-*N *formalism*

The large-N approach for the t-J model was originally developed in Ref. [88], and extensively used in the context of charge excitations in cuprates, among others, Refs. [28,29,32,50,86,89–91]. The aim of this section is to give a brief description of the main formulas.

The layered t-J-V model is written as

$$H = -\sum_{i,j,\sigma} t_{ij} \tilde{c}_{i\sigma}^{\dagger} \tilde{c}_{j\sigma} + \sum_{\langle i,j\rangle} J_{ij} \left(\vec{S}_i \cdot \vec{S}_j - \frac{1}{4} n_i n_j \right) + \sum_{\langle i,j\rangle} V_{ij} n_i n_j, \tag{13}$$

where the sites i and j run over a three-dimensional lattice. The hopping t_{ij} takes a value t, t', and t'' between the first, second, and third nearest-neighbor sites on a square lattice, respectively. The hopping integral between layers is scaled by t_z (see later for the specific form of the electronic dispersion). $\langle i, j\rangle$ denotes a nearest-neighbor pair of sites. The exchange interaction $J_{ij} = J$ is considered only inside the plane; the exchange term between the planes ($J_{\perp}$) is much smaller than J [92]. V_{ij} is the long-range Coulomb interaction on the lattice and is given in momentum space by Eq. (8). $\tilde{c}_{i\sigma}^{\dagger}$ ($\tilde{c}_{i\sigma}$) is the creation (annihilation) operator of electrons with spin $\sigma = (\uparrow, \downarrow)$ in the Fock space without double occupancy. $n_i = \sum_{\sigma} \tilde{c}_{i\sigma}^{\dagger} \tilde{c}_{i\sigma}$ is the electron density operator and $\vec{S}_i$ is the spin operator.

In the large-N theory [28] the electronic dispersion $E_{\mathbf{k}}$ reads

$$E_{\mathbf{k}} = E_{\mathbf{k}}^{\parallel} + E_{\mathbf{k}}^{\perp}, \tag{14}$$

where

$$E_{\mathbf{k}}^{\parallel} = -2\left(t\frac{\delta}{2} + \Delta\right)(\cos k_x + \cos k_y) - 4t'\frac{\delta}{2}\cos k_x \cos k_y - 2t''\frac{\delta}{2}(\cos 2k_x + \cos 2k_y) - \mu, \tag{15}$$

$$E_{\mathbf{k}}^{\perp} = -\frac{t_z}{4}\frac{\delta}{2}(\cos k_x - \cos k_y)^2 \cos k_z. \tag{16}$$

For a given doping δ, the chemical potential μ and Δ are determined self-consistently by solving

$$\Delta = \frac{J}{4N_s} \sum_{\mathbf{k}} (\cos k_x + \cos k_y) n_F(E_{\mathbf{k}}), \tag{17}$$

and

$$(1 - \delta) = \frac{2}{N_s} \sum_{\mathbf{k}} n_F(E_{\mathbf{k}}). \tag{18}$$

We have obtained for $\delta = 0.16$ the values $\mu = -0.044\,\text{eV}$ and $\Delta = 0.024\,\text{eV}$ for LSCO, and $\mu = -0.010\,\text{eV}$ and $\Delta = 0.024\,\text{eV}$ for LCCO.

In the context of the t-J model using a path-integral representation [88] for Hubbard operators [93], a six-component bosonic field is defined as

$$\delta X^a = (\delta R,\ \delta\lambda,\ r^x,\ r^y,\ A^x,\ A^y), \tag{19}$$

where δR describes fluctuations of the number of holes at each site, thus, it is related to on-site charge fluctuations, $\delta\lambda$ is the fluctuation of the Lagrange multiplier introduced to enforce the constraint that prohibits the double occupancy at any site, and r^x and r^y (A^x and A^y) describe fluctuations of the real (imaginary) part of the bond field from the J term.

The inverse of the 6×6 bare bosonic propagator associated with δX^a is

$$\left[D_{ab}^{(0)}(\mathbf{q}, \mathrm{i}\omega_n)\right]^{-1} = N \begin{pmatrix} \frac{\delta^2}{2}[V(\mathbf{q}) - J(\mathbf{q})] & \delta/2 & 0 & 0 & 0 & 0 \\ \delta/2 & 0 & 0 & 0 & 0 & 0 \\ 0 & 0 & \frac{4}{J}\Delta^2 & 0 & 0 & 0 \\ 0 & 0 & 0 & \frac{4}{J}\Delta^2 & 0 & 0 \\ 0 & 0 & 0 & 0 & \frac{4}{J}\Delta^2 & 0 \\ 0 & 0 & 0 & 0 & 0 & \frac{4}{J}\Delta^2 \end{pmatrix}, \tag{20}$$

where $J(\mathbf{q}) = \frac{J}{2}(\cos q_x + \cos q_y)$. We use $J/t = 0.3$.

At leading order, the bare propagator $D_{ab}^{(0)}$ is renormalized in $O(1/N)$. From the Dyson equation the renormalized bosonic propagator is

$$[D_{ab}(\mathbf{q}, \mathrm{i}\omega_n)]^{-1} = \left[D_{ab}^{(0)}(\mathbf{q}, \mathrm{i}\omega_n)\right]^{-1} - \Pi_{ab}(\mathbf{q}, \mathrm{i}\omega_n). \tag{21}$$

Here, the 6×6 boson self-energy matrix Π_{ab} is

$$\Pi_{ab}(\mathbf{q}, \mathrm{i}\omega_n) = -\frac{N}{N_s} \sum_{\mathbf{k}} h_a(\mathbf{k}, \mathbf{q}, E_{\mathbf{k}} - E_{\mathbf{k}-\mathbf{q}}) \times \frac{n_F(E_{\mathbf{k}-\mathbf{q}}) - n_F(E_{\mathbf{k}})}{\mathrm{i}\omega_n - E_{\mathbf{k}} + E_{\mathbf{k}-\mathbf{q}}} h_b(\mathbf{k}, \mathbf{q}, E_{\mathbf{k}} - E_{\mathbf{k}-\mathbf{q}}) - \delta_{a1}\delta_{b1} \frac{N}{N_s} \sum_{\mathbf{k}} \frac{\tilde{E}_{\mathbf{k}-\mathbf{q}} - \tilde{E}_{\mathbf{k}}}{2} n_F(E_{\mathbf{k}}), \tag{22}$$

where $\tilde{E}_{\mathbf{k}}$ is equal to $E_{\mathbf{k}}$ with $\Delta = 0$ and the six-component interaction vertex is given by

$$h_a(\mathbf{k},\mathbf{q},\nu) = \Bigg\{ \frac{2E_{\mathbf{k}-\mathbf{q}} + \nu + 2\mu}{2} + 2\Delta\Bigg[\cos\left(k_x - \frac{q_x}{2}\right)\cos\left(\frac{q_x}{2}\right) + \cos\left(k_y - \frac{q_y}{2}\right)\cos\left(\frac{q_y}{2}\right)\Bigg]; 1; -2\Delta\cos\left(k_x - \frac{q_x}{2}\right); -2\Delta\cos\left(k_y - \frac{q_y}{2}\right); 2\Delta\sin\left(k_x - \frac{q_x}{2}\right); 2\Delta\sin\left(k_y - \frac{q_y}{2}\right)\Bigg\}. \quad (23)$$

In the writing of this manuscript we noted a misprint in the last term of of Eq. (22) in previous works, which has been corrected here.

As discussed previously [88,89], the element (1,1) of D_{ab} is related to the usual charge-charge correlation function $\chi_{tJV}(\mathbf{r}_i - \mathbf{r}_j, \tau) = \langle T_\tau n_i(\tau) n_j(0)\rangle$, which in the large-$N$ scheme is computed in the $\mathbf{q}$-ω space as

$$\chi_{\mathrm{tJV}}(\mathbf{q}, \mathrm{i}\omega_n) = N\left(\frac{\delta}{2}\right)^2 D_{11}(\mathbf{q}, \mathrm{i}\omega_n). \quad (24)$$

It is important to remark that the charge-charge correlation function is nearly unaffected by the value of J [77]. As for $\chi_{\mathrm{RPA}}(\mathbf{q}, \mathrm{i}\omega_n)$, after performing the analytical continuation $\mathrm{i}\omega_n \to \omega + \mathrm{i}\Gamma$ in $\chi_{\mathrm{tJV}}(\mathbf{q}, \mathrm{i}\omega_n)$ we obtain the imaginary part of the charge-charge correlation functions $\chi''_{\mathrm{tJV}}(\mathbf{q}, \omega)$. The plasmon excitations are obtained for the resonant peaks of $\chi''_{\mathrm{tJV}}(\mathbf{q}, \omega)$.

4. *Correlations in the* t-J-V *and RPA models*

Looking at the large-N formalism in Sec. V B 3, it is not clear why the plasmon excitations obtained in the context of the t-J-V model are similar to those obtained in RPA. Although the large-N formalism for the t-J-V model seems to be complicated and rather different from the usual RPA, here we show that inside this framework an RPA structure is contained. The large-N formalism within the t-J-V model renormalizes the band parameters due to electron correlations, which can be seen in the band dispersion directly [Eqs. (14)–(16)]. Comparing it to the usual tight-binding dispersion [Eqs. (4)–(6)], we obtain

$$\begin{aligned} t_{\mathrm{eff}} &= t\delta + \Delta, \\ t'_{\mathrm{eff}} &= t'\delta, \\ t''_{\mathrm{eff}} &= t''\delta, \\ t_{z_{\mathrm{eff}}} &= t_z\delta, \end{aligned} \quad (25)$$

where the hopping parameters t, t', t'', and t_z are the tight-binding bare ones. We introduced these effective parameters into the RPA model and plotted the obtained plasmon dispersion in Fig. 5. To understand the deviation at large momenta between RPA and t-J-V, we consider only the 2×2 sector ($a, b = 1, 2$) in the $D_{ab}(\mathbf{q}, \mathrm{i}\omega_n)$ [Eq. (21)]. If in Eq. (21) we set manually the bosonic self-energy components Π_{11} and Π_{12} to zero, the only relevant component is Π_{22}, and from Eqs. (22) and (23) it can be written as

$$\begin{aligned} \Pi_{22}(\mathbf{q}, \mathrm{i}\omega_n) &= -N\sum_{\mathbf{k}} \frac{n_F(E_{\mathbf{k}-\mathbf{q}}) - n_F(E_{\mathbf{k}})}{\mathrm{i}\omega_n - E_{\mathbf{k}} + E_{\mathbf{k}-\mathbf{q}}} \\ &= -N\frac{\chi_0(\mathbf{q}, \mathrm{i}\omega_n)}{2}. \end{aligned} \quad (26)$$

In spite of χ_0 [Eq. (11)] representing the particle-hole continuum within the RPA and Π_{22} appearing in the large-N formalism within the t-J-V model as only one component of the bosonic self-energy carrying the information of the fluctuations of the Lagrange multiplier associated with the constraint that prohibits the double occupancy, both have a similar mathematical form. In this context, we compute $\chi_{\mathrm{tJV}}(\mathbf{q}, \mathrm{i}\omega_n)$ in Eq. (24) using the physical value $N = 2$ [28], which gives

$$\chi_{\mathrm{tJV}}(\mathbf{q}, \mathrm{i}\omega_n) = \frac{\chi_0(\mathbf{q}, \mathrm{i}\omega_n)}{1 - V'(\mathbf{q})\chi_0(\mathbf{q}, \mathrm{i}\omega_n)}, \quad (27)$$

where $V'(\mathbf{q}) = 2[V(\mathbf{q}) - J(\mathbf{q})]$. Equation (27) shows that the charge-charge correlation function in the large-N formalism considering only the contribution from Π_{22} has an RPA-like mathematical form. This shows the presence of a "hidden" RPA structure with electronic correlations within the t-J-V formalism with respect to RPA. The contribution of $J(\mathbf{q})$ can be neglected because $V(\mathbf{q})$ is significantly larger, and the factor 2 accounts for the transformation to electron volts using the renormalized value of t in the large-N formalism. In fact, this supports the picture that the effective mass m^* introduced in RPA has an electronic correlated origin.

ACKNOWLEDGMENTS

We thank A. A. Aligia, M. Hepting, C. Falter and W. S. Lee for discussions and comments. The RIXS experiments were primarily supported by user research program of Diamond Light Source, Ltd., U.K. through beam-time Proposal No. MM27872. A part of the results presented in this work was obtained by using the facilities of the CCT-Rosario Computational Center, member of the High Performance Computing National System (SNCAD, MincyT-Argentina). J.C. acknowledges financial support from the National Research Foundation of Korea (NRF) funded by the Korean government (MSIT) through Sejong Science Fellowship (Grant No. RS-2023-00252768). A.N. acknowledges the Marie Skłodowska-Curie Grant Agreement No. 884104 (PSI-FELLOW-III-3i). H.Y. was supported by JSPS KAKENHI Grant No. JP20H01856 and World Premier International Research Center Initiative (WPI), MEXT, Japan. Z.L. acknowledges the National Natural Science Foundation of China (12225412), and CAS Project for Young Scientists in Basic Research (2022YSBR-048).

[1] C. Proust and L. Taillefer, The remarkable underlying ground states of cuprate superconductors, Annu. Rev. Condens. Matter Phys. **10**, 409 (2019).

[2] B. Keimer, S. A. Kivelson, M. R. Norman, S. Uchida, and J. Zaanen, From quantum matter to high-temperature superconductivity in copper oxides, Nature (London) **518**, 179 (2015).

[3] A. Kaiser, A. Snezhko, and I. S. Aranson, Flocking ferromagnetic colloids, Sci. Adv. **3**, e1601469 (2017).

[4] D. R. Chialvo, Emergent complex neural dynamics, Nat. Phys. **6**, 744 (2010).

[5] D. Pines and D. Bohm, A collective description of electron interactions: II. Collective vs. individual particle aspects of the interactions, Phys. Rev. **85**, 338 (1952).

[6] I. Bozovic, Plasmons in cuprate superconductors, Phys. Rev. B **42**, 1969 (1990).

[7] A. L. Fetter, Electrodynamics of a layered electron gas. II. Periodic array, Ann. Phys. **88**, 1 (1974).

[8] M. Apostol, Plasma frequency of the electron gas in layered structures, Z. Phys. B **22**, 13 (1975).

[9] R. S. Markiewicz, M. Z. Hasan, and A. Bansil, Acoustic plasmons and doping evolution of Mott physics in resonant inelastic x-ray scattering from cuprate superconductors, Phys. Rev. B **77**, 094518 (2008).

[10] D. Grecu, Plasma frequency of the electron gas in layered structures, Phys. Rev. B **8**, 1958 (1973).

[11] N. Nücker, H. Romberg, S. Nakai, B. Scheerer, J. Fink, Y. F. Yan, and Z. X. Zhao, Plasmons and interband transitions in $Bi_2Sr_2CaCu_2O_8$, Phys. Rev. B **39**, 12379(R) (1989).

[12] M. Hepting, L. Chaix, E. W. Huang, R. Fumagalli, Y. Y. Peng, B. Moritz, K. Kummer, N. B. Brookes, W. C. Lee, M. Hashimoto, T. Sarkar, J.-F. He, C. R. Rotundu, Y. S. Lee, R. L. Greene, L. Braicovich, G. Ghiringhelli, Z. X. Shen, T. P. Devereaux, and W. S. Lee, Three-dimensional collective charge excitations in electron-doped copper oxide superconductors, Nature (London) **563**, 374 (2018).

[13] J. Lin, J. Yuan, K. Jin, Z. Yin, G. Li, K.-J. Zhou, X. Lu, M. Dantz, T. Schmitt, H. Ding, H. Guo, M. P. M. Dean, and X. Liu, Doping evolution of the charge excitations and electron correlations in electron-doped superconducting $La_{2-x}Ce_xCuO_4$, npj Quantum Mater. **5**, 4 (2020).

[14] A. Singh, H. Y. Huang, C. Lane, J. H. Li, J. Okamoto, S. Komiya, R. S. Markiewicz, A. Bansil, T. K. Lee, A. Fujimori, C. T. Chen, and D. J. Huang, Acoustic plasmons and conducting carriers in hole-doped cuprate superconductors, Phys. Rev. B **105**, 235105 (2022).

[15] M. Hepting *et al.*, Evolution of plasmon excitations across the phase diagram of the cuprate superconductor $La_{2-x}Sr_xCuO_4$, Phys. Rev. B **107**, 214516 (2023).

[16] Q. Li, L. Ju, H. Huang, Y. Zhang, C. Zou, T. Ren, A. Singh, S. Zhang, Q. Qiu, Q. Xiao, D.-J. Huang, Y. Xie, Z. Chen, and Y. Peng, Charge redistribution, charge order and plasmon in $La_{2-x}Sr_xCuO_4/La_2CuO_4$ superlattices, arXiv:2309.01649.

[17] M. Bejas, V. Zimmermann, D. Betto, T. D. Boyko, R. J. Green, T. Loew, N. B. Brookes, G. Cristiani, G. Logvenov, M. Minola, B. Keimer, H. Yamase, A. Greco, and M. Hepting, Plasmon dispersion in bilayer cuprate superconductors, Phys. Rev. B **109**, 144516 (2024).

[18] V. Z. Kresin and H. Morawitz, Layer plasmons and high-T_c superconductivity, Phys. Rev. B **37**, 7854 (1988).

[19] J. Levallois, M. K. Tran, D. Pouliot, C. N. Presura, L. H. Greene, J. N. Eckstein, J. Uccelli, E. Giannini, G. D. Gu, A. J. Leggett, and D. van der Marel, Temperature-dependent ellipsometry measurements of partial Coulomb energy in superconducting cuprates, Phys. Rev. X **6**, 031027 (2016).

[20] A. Bill, H. Morawitz, and V. Z. Kresin, Electronic collective modes and superconductivity in layered conductors, Phys. Rev. B **68**, 144519 (2003).

[21] T. Bauer and C. Falter, Impact of dynamical screening on the phonon dynamics of metallic La_2CuO_4, Phys. Rev. B **80**, 094525 (2009).

[22] C. Falter and M. Klenner, Nonadiabatic and nonlocal electron-phonon interaction and phonon-plasmon mixing in the high-temperature superconductors, Phys. Rev. B **50**, 9426 (1994).

[23] G. Dellea, M. Minola, A. Galdi, D. Di Castro, C. Aruta, N. B. Brookes, C. J. Jia, C. Mazzoli, M. Moretti Sala, B. Moritz, P. Orgiani, D. G. Schlom, A. Tebano, G. Balestrino, L. Braicovich, T. P. Devereaux, L. Maritato, and G. Ghiringhelli, Spin and charge excitations in artificial hole- and electron-doped infinite layer cuprate superconductors, Phys. Rev. B **96**, 115117 (2017).

[24] D. Meyers, H. Miao, A. C. Walters, V. Bisogni, R. S. Springell, M. d'Astuto, M. Dantz, J. Pelliciari, H. Y. Huang, J. Okamoto, D. J. Huang, J. P. Hill, X. He, I. Božović, T. Schmitt, and M. P. M. Dean, Doping dependence of the magnetic excitations in $La_{2-x}Sr_xCuO_4$, Phys. Rev. B **95**, 075139 (2017).

[25] H. C. Robarts, M. Barthélemy, K. Kummer, M. García-Fernández, J. Li, A. Nag, A. C. Walters, K. J. Zhou, and S. M. Hayden, Anisotropic damping and wave vector dependent susceptibility of the spin fluctuations in $La_{2-x}Sr_xCuO_4$ studied by resonant inelastic x-ray scattering, Phys. Rev. B **100**, 214510 (2019).

[26] J. Spałek, M. Fidrysiak, M. Zegrodnik, and A. Biborski, Superconductivity in high- T_c and related strongly correlated systems from variational perspective: Beyond mean field theory, Phys. Rep. **959**, 1 (2022).

[27] M. Fidrysiak and J. Spałek, A unified theory of spin and charge excitations in high-T_c cuprates: Quantitative comparison with experiment and interpretation, Phys. Rev. B **104**, L020510 (2021).

[28] A. Greco, H. Yamase, and M. Bejas, Plasmon excitations in layered high-T_c cuprates, Phys. Rev. B **94**, 075139 (2016).

[29] A. Greco, H. Yamase, and M. Bejas, Origin of high-energy charge excitations observed by resonant inelastic x-ray scattering in cuprate superconductors, Commun. Phys. **2**, 3 (2019).

[30] R. Comin and A. Damascelli, ARPES: A probe of electronic correlations, in *Strongly Correlated Systems: Experimental Techniques*, edited by A. Avella and F. Mancini (Springer, Berlin, Heidelberg, 2015), pp. 31–71.

[31] N. Nücker, U. Eckern, J. Fink, and P. Müller, Long-wavelength collective excitations of charge carriers in high-T_c superconductors, Phys. Rev. B **44**, 7155 (1991).

[32] A. Nag, M. Zhu, M. Bejas, J. Li, H. C. Robarts, H. Yamase, A. N. Petsch, D. Song, H. Eisaki, A. C. Walters, M. García-Fernández, A. Greco, S. M. Hayden, and K.-J. Zhou, Detection of acoustic plasmons in hole-doped lanthanum and bismuth cuprate superconductors using resonant inelastic x-ray scattering, Phys. Rev. Lett. **125**, 257002 (2020).

[33] P. Prelovšek and P. Horsch, Electron-energy loss spectra and plasmon resonance in cuprates, Phys. Rev. B **60**, R3735 (1999).

[34] M. Mitrano, A. A. Husain, S. Vig, A. Kogar, M. S. Rak, S. I. Rubeck, J. Schmalian, B. Uchoa, J. Schneeloch, R. Zhong, G. D. Gu, and P. Abbamonte, Anomalous density fluctuations in a strange metal, Proc. Natl. Acad. Sci. USA **115**, 5392 (2018).

[35] A. A. Husain, M. Mitrano, M. S. Rak, S. Rubeck, B. Uchoa, K. March, C. Dwyer, J. Schneeloch, R. Zhong, G. D. Gu, and P. Abbamonte, Crossover of charge fluctuations across the strange metal phase diagram, Phys. Rev. X **9**, 041062 (2019).

[36] A. Romero-Bermúdez, A. Krikun, K. Schalm, and J. Zaanen, Anomalous attenuation of plasmons in strange metals and holography, Phys. Rev. B **99**, 235149 (2019).

[37] B. Moritz, F. Schmitt, W. Meevasana, S. Johnston, E. M. Motoyama, M. Greven, D. H. Lu, C. Kim, R. T. Scalettar, Z.-X. Shen, and T. P. Devereaux, Effect of strong correlations on the high energy anomaly in hole- and electron-doped high-T_c superconductors, New J. Phys. **11**, 093020 (2009).

[38] H. Das and T. Saha-Dasgupta, Electronic structure of La_2CuO_4 in the T and T' crystal structures using dynamical mean field theory, Phys. Rev. B **79**, 134522 (2009).

[39] C. Weber, K. Haule, and G. Kotliar, Apical oxygens and correlation strength in electron- and hole-doped copper oxides, Phys. Rev. B **82**, 125107 (2010).

[40] P. A. Lee, N. Nagaosa, and X.-G. Wen, Doping a Mott insulator: Physics of high-temperature superconductivity, Rev. Mod. Phys. **78**, 17 (2006).

[41] J. Zaanen, G. A. Sawatzky, and J. W. Allen, Band gaps and electronic structure of transition-metal compounds, Phys. Rev. Lett. **55**, 418 (1985).

[42] V. J. Emery, Theory of high-T_c superconductivity in oxides, Phys. Rev. Lett. **58**, 2794 (1987).

[43] C. Varma, S. Schmitt-Rink, and E. Abrahams, Charge transfer excitations and superconductivity in "ionic" metals, Solid State Commun. **62**, 681 (1987).

[44] C. T. Chen, F. Sette, Y. Ma, M. S. Hybertsen, E. B. Stechel, W. M. C. Foulkes, M. Schulter, S.-W. Cheong, A. S. Cooper, L. W. Rupp, B. Batlogg, Y. L. Soo, Z. H. Ming, A. Krol, and Y. H. Kao, Electronic states in $La_{2-x}Sr_xCuO_{4+\delta}$ probed by soft-x-ray absorption, Phys. Rev. Lett. **66**, 104 (1991).

[45] N. P. Armitage, P. Fournier, and R. L. Greene, Progress and perspectives on electron-doped cuprates, Rev. Mod. Phys. **82**, 2421 (2010).

[46] J. Fink, N. Nücker, E. Pellegrin, H. Romberg, M. Alexander, and M. Knupfer, Electron energy-loss and x-ray absorption spectroscopy of cuprate superconductors and related compounds, J. Electron. Spectrosc. Relat. Phenom. **66**, 395 (1994).

[47] E. Pellegrin, N. Nücker, J. Fink, S. L. Molodtsov, A. Gutiérrez, E. Navas, O. Strebel, Z. Hu, M. Domke, G. Kaindl, S. Uchida, Y. Nakamura, J. Markl, M. Klauda, G. Saemann-Ischenko, A. Krol, J. L. Peng, Z. Y. Li, and R. L. Greene, Orbital character of states at the Fermi level in $La_{2-x}Sr_xCuO_4$ and $R_{2-x}Ce_xCuO_4$ (R=Nd, Sm), Phys. Rev. B **47**, 3354 (1993).

[48] H. Miao, J. Lorenzana, G. Seibold, Y. Y. Peng, A. Amorese, F. Yakhou-Harris, K. Kummer, N. B. Brookes, R. M. Konik, V. Thampy, G. D. Gu, G. Ghiringhelli, L. Braicovich, and M. P. M. Dean, High-temperature charge density wave correlations in $La_{1.875}Ba_{0.125}CuO_4$ without spin–charge locking, Proc. Natl. Acad. Sci. USA **114**, 12430 (2017).

[49] W. S. Lee, J. J. Lee, E. A. Nowadnick, S. Gerber, W. Tabis, S. W. Huang, V. N. Strocov, E. M. Motoyama, G. Yu, B. Moritz, H. Y. Huang, R. P. Wang, Y. B. Huang, W. B. Wu, C. T. Chen, D. J. Huang, M. Greven, T. Schmitt, Z. X. Shen, and T. P. Devereaux, Asymmetry of collective excitations in electron- and hole-doped cuprate superconductors, Nat. Phys. **10**, 883 (2014).

[50] M. Hepting, M. Bejas, A. Nag, H. Yamase, N. Coppola, D. Betto, C. Falter, M. Garcia-Fernandez, S. Agrestini, K.-J. Zhou, M. Minola, C. Sacco, L. Maritato, P. Orgiani, H. Wei, K. Shen, D. Schlom, A. Galdi, A. Greco, and B. Keimer, Gapped collective charge excitations and interlayer hopping in cuprate superconductors, Phys. Rev. Lett. **129**, 047001 (2022).

[51] S. Uchida, T. Ido, H. Takagi, T. Arima, Y. Tokura, and S. Tajima, Optical spectra of $La_{2-x}Sr_xCuO_4$: Effect of carrier doping on the electronic structure of the CuO_2 plane, Phys. Rev. B **43**, 7942 (1991).

[52] R. S. Markiewicz, S. Sahrakorpi, M. Lindroos, H. Lin, and A. Bansil, One-band tight-binding model parametrization of the high- T_c cuprates including the effect of k_z dispersion, Phys. Rev. B **72**, 054519 (2005).

[53] J. Fink, M. Knupfer, S. Atzkern, and M. Golden, Electronic correlations in solids, studied using electron energy-loss spectroscopy, J. Electron. Spectrosc. Relat. Phenom. **117-118**, 287 (2001).

[54] V. G. Grigoryan, G. Paasch, and S.-L. Drechsler, Determination of an effective one-electron spectrum from the plasmon dispersion of nearly optimally doped $Bi_2Sr_2CaCu_2O_8$, Phys. Rev. B **60**, 1340 (1999).

[55] M. Knupfer, F. Jerzembeck, N. Kikugawa, F. Roth, and J. Fink, Propagating charge carrier plasmon in Sr_2RuO_4, Phys. Rev. B **106**, L241103 (2022).

[56] J. Schultz, A. Lubk, F. Jerzembeck, N. Kikugawa, M. Knupfer, D. Wolf, B. Büchner, and J. Fink, Optical and acoustic plasmons in the layered material Sr_2RuO_4, arXiv:2401.05880.

[57] D. Stricker, J. Mravlje, C. Berthod, R. Fittipaldi, A. Vecchione, A. Georges, and D. van der Marel, Optical response of Sr_2RuO_4 reveals universal Fermi-liquid scaling and quasiparticles beyond Landau theory, Phys. Rev. Lett. **113**, 087404 (2014).

[58] X. Deng, J. Mravlje, R. Žitko, M. Ferrero, G. Kotliar, and A. Georges, How bad metals turn good: Spectroscopic signatures of resilient quasiparticles, Phys. Rev. Lett. **110**, 086401 (2013).

[59] A. Ino, C. Kim, M. Nakamura, T. Yoshida, T. Mizokawa, A. Fujimori, Z.-X. Shen, T. Kakeshita, H. Eisaki, and S. Uchida, Doping-dependent evolution of the electronic structure of $La_{2-x}Sr_xCuO_4$ in the superconducting and metallic phases, Phys. Rev. B **65**, 094504 (2002).

[60] C. Weber, K. Haule, and G. Kotliar, Strength of correlations in electron- and hole-doped cuprates, Nat. Phys. **6**, 574 (2010).

[61] A. Kobayashi, A. Tsuruta, T. Matsuura, and Y. Kuroda, The electron–hole asymmetry in the cuprate superconductors, Physica C **388-389**, 39 (2003).

[62] K. Segawa, M. Kofu, S.-H. Lee, I. Tsukada, H. Hiraka, M. Fujita, S. Chang, K. Yamada, and Y. Ando, Zero-doping state and electron–hole asymmetry in an ambipolar cuprate, Nat. Phys. **6**, 579 (2010).

[63] R. Mizuno, M. Ochi, and K. Kuroki, DMFT study on the electron–hole asymmetry of the electron correlation strength in the high T_c cuprates, J. Phys. Soc. Jpn. **86**, 114706 (2017).

[64] D. Ogura and K. Kuroki, Asymmetry of superconductivity in hole- and electron-doped cuprates: Explanation within two-particle self-consistent analysis for the three-band model, Phys. Rev. B **92**, 144511 (2015).

[65] L. de' Medici, X. Wang, M. Capone, and A. J. Millis, Correlation strength, gaps, and particle-hole asymmetry in high-T_c cuprates: A dynamical mean field study of the three-band copper-oxide model, Phys. Rev. B **80**, 054501 (2009).

[66] D. F. DuBois and M. G. Kivelson, Electron correlational effects on plasmon damping and ultraviolet absorption in metals, Phys. Rev. **186**, 409 (1969).

[67] L. E. Oliveira and K. Sturm, High-frequency dielectric properties of covalent semiconductors within the nearly-free-electron approximation. II. The two-plasmon-band model, Phys. Rev. B **22**, 6283 (1980).

[68] K. Sturm, Electron energy loss in simple metals and semiconductors, Adv. Phys. **31**, 1 (1982).

[69] G. Paasch, Influence of interband transitions on plasmons in the alkali metals; pseudopotential calculation, Phys. Status Solidi B **38**, A123 (1970).

[70] P. C. Gibbons and S. E. Schnatterly, Comment on the line shape of the plasma resonance in simple metals, Phys. Rev. B **15**, 2420 (1977).

[71] A. vom Felde, J. Sprösser-Prou, and J. Fink, Valence-electron excitations in the alkali metals, Phys. Rev. B **40**, 10181 (1989).

[72] J. J. Ritsko, Valence- and core-electronic excitations in potassium-intercalated graphite, Phys. Rev. B **25**, 6452 (1982).

[73] H. Hafermann, E. G. C. P. van Loon, M. I. Katsnelson, A. I. Lichtenstein, and O. Parcollet, Collective charge excitations of strongly correlated electrons, vertex corrections, and gauge invariance, Phys. Rev. B **90**, 235105 (2014).

[74] A. Hunter, S. Beck, E. Cappelli, F. Margot, M. Straub, Y. Alexanian, G. Gatti, M. D. Watson, T. K. Kim, C. Cacho, N. C. Plumb, M. Shi, M. Radović, D. A. Sokolov, A. P. Mackenzie, M. Zingl, J. Mravlje, A. Georges, F. Baumberger, and A. Tamai, Fate of quasiparticles at high temperature in the correlated metal Sr_2RuO_4, Phys. Rev. Lett. **131**, 236502 (2023).

[75] B. Michon, C. Berthod, C. W. Rischau, A. Ataei, L. Chen, S. Komiya, S. Ono, L. Taillefer, D. van der Marel, and A. Georges, Reconciling scaling of the optical conductivity of cuprate superconductors with Planckian resistivity and specific heat, Nat. Commun. **14**, 3033 (2023).

[76] G. Khaliullin and P. Horsch, Theory of the density fluctuation spectrum of strongly correlated electrons, Phys. Rev. B **54**, R9600 (1996).

[77] M. Bejas, H. Yamase, and A. Greco, Dual structure in the charge excitation spectrum of electron-doped cuprates, Phys. Rev. B **96**, 214513 (2017).

[78] M. Zafur and H. Yamase, Spin and bond-charge excitation spectra in correlated electron systems near an antiferromagnetic phase, Phys. Rev. B **109**, 245127 (2024).

[79] F. Roth, A. Revcolevschi, B. Büchner, M. Knupfer, and J. Fink, Evidence for an orbital dependent Mott transition in the ladders of $(La, Ca)_xSr_{14-x}Cu_{24}O_{41}$ derived by electron energy loss spectroscopy, Phys. Rev. B **101**, 195132 (2020).

[80] J. Yuan *et al.*, Scaling of the strange-metal scattering in unconventional superconductors, Nature (London) **602**, 431 (2022).

[81] A. Sawa, M. Kawasaki, H. Takagi, and Y. Tokura, Electron-doped superconductor $La_{2-x}Ce_xCuO_4$: Preparation of thin films and modified doping range for superconductivity, Phys. Rev. B **66**, 014531 (2002).

[82] K.-J. Zhou, A. Walters, M. Garcia-Fernandez, T. Rice, M. Hand, A. Nag, J. Li, S. Agrestini, P. Garland, H. Wang, S. Alcock, I. Nistea, B. Nutter, N. Rubies, G. Knap, M. Gaughran, F. Yuan, P. Chang, J. Emmins, and G. Howell, I21: an advanced high-resolution resonant inelastic X-ray scattering beamline at Diamond Light Source, J. Synchrotron Radiat. **29**, 563 (2022).

[83] A. L. Fetter, Electrodynamics of a layered electron gas. I. Single layer, Ann. Phys. **81**, 367 (1973).

[84] F. Becca, M. Tarquini, M. Grilli, and C. Di Castro, Charge-density waves and superconductivity as an alternative to phase separation in the infinite-U Hubbard-Holstein model, Phys. Rev. B **54**, 12443 (1996).

[85] G. D. Mahan, *Many-Particle Physics* (Springer US, Boston, 1990).

[86] A. Greco, H. Yamase, and M. Bejas, Close inspection of plasmon excitations in cuprate superconductors, Phys. Rev. B **102**, 024509 (2020).

[87] A. A. Zabolotnykh and V. A. Volkov, Plasmons and magnetoplasmons in partially bounded two-layer electron systems, Phys. Rev. B **102**, 165306 (2020).

[88] A. Foussats and A. Greco, Large-N expansion based on the Hubbard operator path integral representation and its application to the t-J model. II. The case for finite J, Phys. Rev. B **70**, 205123 (2004).

[89] M. Bejas, A. Greco, and H. Yamase, Possible charge instabilities in two-dimensional doped Mott insulators, Phys. Rev. B **86**, 224509 (2012).

[90] H. Yamase, M. Bejas, and A. Greco, Electron self-energy from quantum charge fluctuations in the layered t-J model with long-range Coulomb interaction, Phys. Rev. B **104**, 045141 (2021).

[91] H. Yamase, M. Bejas, and A. Greco, Plasmarons in high-temperature cuprate superconductors, Commun. Phys. **6**, 168 (2023).

[92] T. Thio, T. R. Thurston, N. W. Preyer, P. J. Picone, M. A. Kastner, H. P. Jenssen, D. R. Gabbe, C. Y. Chen, R. J. Birgeneau, and A. Aharony, Antisymmetric exchange and its influence on the magnetic structure and conductivity of La_2CuO_4, Phys. Rev. B **38**, 905 (1988).

[93] J. Hubbard, Electron correlations in narrow energy bands, Proc. R. Soc. London A **276**, 238 (1963).